J Mater Sci: Mater Med (2010) 21:515–523
DOI 10.1007/s10856-009-3906-y

Biomimetic calcium phosphate coating on Ti wires versus flat substrates: structure and mechanism of formation

Tal Reiner · Irena Gotman

Received: 16 July 2009 / Accepted: 5 October 2009 / Published online: 23 October 2009

Abstract Biomimetic calcium phosphate (Ca–P) coatings improve the osteoconductivity of orthopedic implants and show promise as slow delivery systems for growth factors. This paper compares the structure and composition of biomimetic coatings on flat titanium coupons and on Ti wires/thin pins that are often used as model implants in small animal in vivo models. Ca–P coatings were grown on alkali-treated Ti substrates using a two-step deposition procedure. The coatings on wires consisted of a surface layer of octacalcium phosphate (OCP) and a layer of Ca-deficient hydroxyapatite (CDHA) underneath. The coating thickness and the proportion of CDHA decreased with increasing wire diameter. The coatings on flat coupons were the thinnest, and were comprised almost entirely of OCP. A mechanism of successive formation of the CDHA and OCP phases based on the interplay between nucleation, growth and hydrolysis of OCP crystals as a function of changing local supersaturation is proposed.

1 Introduction

Ca–P coatings are often applied onto the surface of orthopedic implants made of titanium alloys in order to enhance bone bonding and subsequent fixation of the implant [1, 2]. A method widely used for the deposition of Ca–P layers (mostly hydroxyapatite, HA) is plasma spraying. Being a line-of-sight method, however, plasma spraying is unsuitable for coating complex-shape and porous implants. Moreover, the high temperatures of the process prevent incorporation of drugs and bone-growth stimulating factors into the Ca–P layers. These limitations don't exist in the biomimetic approach where Ca–P coatings are deposited from simulated body fluids at the physiologic temperature and pH. Biomimetic coatings comprising different Ca–P phases (notably hydroxyapatite, HA, and octacalcium phosphate, OCP) were obtained by different groups depending on surface pretreatment and composition of the soaking solutions [3–6]. Given the varying solubilities of different Ca–P compounds, different bone-bonding and bone-healing capabilities may be expected from these coatings.

The group of de Groot has developed a two-step biomimetic coating route where the substrate is immersed successively in 5-times concentrated simulated body fluid (SBF) under high-nucleation conditions, and in a supersaturated solution of calcium phosphate [7–9]. They have demonstrated that such biomimetic coatings grown on flat Ti plates consist of a single-phase OCP layer [7, 8]. The method was also used to coat porous sintered Ti and trabecular Ta bone scaffolds however the influence of substrate geometry on the biomimetic deposition process has not been studied. The 3D structure of a bone scaffold is comprised of thin wires/struts, and the Ca–P coatings formed on wires are not necessarily identical to those on flat surfaces. Moreover, Ti wires/thin pins are used as model implants in in vivo small animal studies. Thus, thin Ti pins are often implanted into rat tibiae or maxillae to evaluate the effect of coatings and other surface modifications on new bone formation and bone bonding around titanium orthopedic and dental implants [10–14]. If a biomimetic coating is to be studied in such rat model, it is paramount to make sure that the Ca–P coating on the small wire/pin rat implant closely replicates the one on the real

T. Reiner · I. Gotman (✉)
Faculty of Materials Engineering, Technion-IIT, Haifa 32000, Israel
e-mail: gotman@tx.technion.ac.il

large scale implant in terms of phase composition and microstructure.

The purpose of the present paper is, therefore, to study Ca–P coatings biomimetically deposited on Ti wires and to show that they differ from the biomimetic coatings grown on flat Ti surfaces. The deposition method developed by de Groot et al. [7] provided a useful starting point for our work, though differences in surface preparation procedure used may alter the coating structure and phase composition. Moreover, in an effort to get a deeper insight into the process of coating formation, deposition from solutions with different pH and Ca^{2+} concentrations was carried out. The Ca–P layers obtained were extensively characterized and a detailed picture of the coating structure on wires and flat surfaces has emerged.

2 Materials and methods

Ti wires (0.2 and 1 mm diameter) and Ti foil (0.2 mm thickness) were purchased from Performance Materials and Alloys Ltd. (NJ, USA). Salts for SBF preparation, HCl, phosphate buffer (pH = 7) and Soybean Trypsin Inhibitor were purchased from Sigma Chemical Co.

Prior to biomimetic coating deposition, all wires and foils were pretreated by soaking in 5 M NaOH at 60°C for 24 h [15, 16]. The surface of the alkali treated wire was characterized by X-ray Photoelectron Spectroscopy, XPS (Thermo VG Scientific Sigma Probe) and Secondary Ion Mass Spectrometry, SIMS depth profile analysis (Cameca ims4f).

Biomimetic calcium phosphate coatings were prepared by first priming the samples in five times concentrated simulated body fluid (SBF1) for 24 h, followed by soaking in SBF2 (2 times concentrated in terms of Ca and P) [7]. The compositions of SBF1 and SBF2 are given in Table 1.

Two types of SBF2 soaking experiments were performed. In Experiment 1, a 40 cm long 0.2-mm-diam. wire, an 8 cm long 1-mm-diam. wire and a 15 × 8.5 mm^2 foil (all having the same surface area of ~250 mm^2), either alkali-treated or alkali-treated + SBF1-primed, were soaked, each one separately, in 50 ml SBF2 at 37°C for 1–24 h. In Experiment 2, a 10 cm long 0.2-mm-diam. wire and a 16 × 18 mm^2 foil (both alkali-treated + SBF1-primed) were immersed together in 50 ml SBF2 at 37°C, for up to 24 h. The latter experiment was also repeated under conditions of continuous stirring at a speed of 50 rpm.

The coated foils and wires were characterized in a high resolution SEM (HRSEM) LEO 982 and by X-ray diffraction (XRD). For coating thickness measurement, foils/wires were carefully cut with sharp scissors. Coating thickness after each treatment was measured in HRSEM, in five different locations on at least two samples. For XRD analysis, an automatic powder Philips PW-1820 diffractometer with a long-focus $Cu_{K\alpha}$ tube operating at 40 kV and 40 mA was used. Step scans were taken with a 0.02° step and a 5 s exposure. Some coatings were mechanically peeled off the wires and characterized by FTIR spectroscopy (Bruker Equinox 55, transmittance mode) using the conventional KBr pellet methodology. The samples were weighed before and after biomimetic deposition, and the coatings' density was calculated based on their weight and thickness (as measured in SEM).

3 Results

3.1 Alkali treatment of Ti substrates

Alkali treatment of Ti wires resulted in the formation of a nano-porous network surface structure, Fig. 1. XPS analysis detected significant amounts of Na and O (in addition to Ti) near the wire surface suggesting the formation of

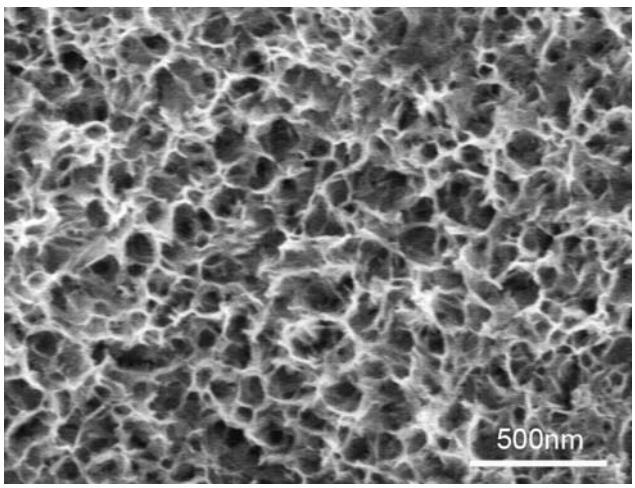

Fig. 1 HRSEM micrograph of alkali treated Ti wire

Table 1 Ionic composition of SBF1 and SBF2 solutions

mM	Na^+	Ca^{2+}	Mg^{2+}	Cl^-	HPO_4^{2-}	HCO_3^-	SO_4^{2-}	pH	Buffer
SBF1	719.9	12.5	7.5	724.0	5.0	21.0	2.5	6.8	
SBF2	140.0	4.0	0.0	144.0	2.0	0.0	0.0	7.2	Tris–HCl

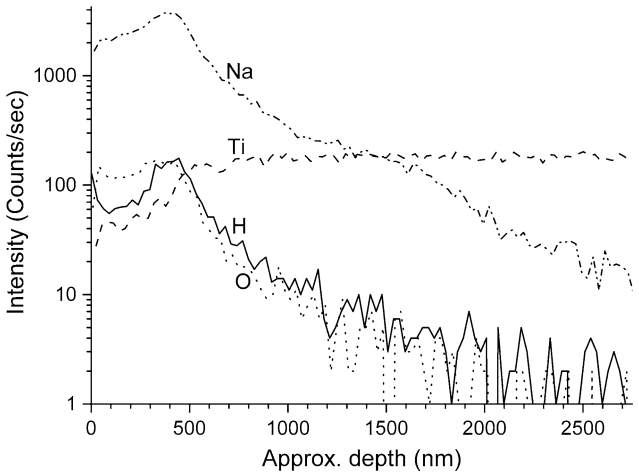

Fig. 2 SIMS depth profile of alkali treated Ti wire, indicating the formation of ~500 nm thick hydroxylated sodium titanate surface layer

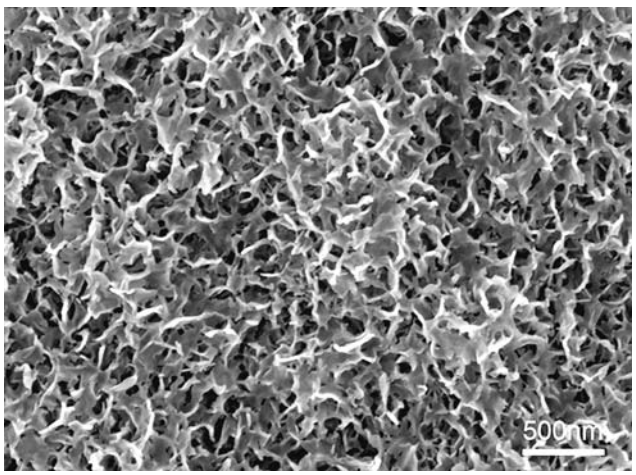

Fig. 3 HRSEM micrographs of Ca–P layer on Ti wire after soaking in SBF1 for 24 h

a sodium titanate hydrogel layer similar to the one reported for alkali-treated flat Ti coupons [16]. According to SIMS depth profiling, Fig. 2, the layer thickness was about 500 nm. Titania hydrogel was reported to be negatively charged in SBF solution thus stimulating Ca–P crystal nucleation by attracting Ca^{2+} ions to the substrate [17]. Moreover, structural similarity has been observed between titania hydrogel and Ca–P layers deposited from SBF1, Fig. 3.

3.2 Priming alkali-treated Ti by soaking in SBF1

HRSEM micrograph in Fig. 3 shows the calcium phosphate layer produced on the surface of the alkali treated Ti wire after 24 h soaking in SBF1. The layer is 3.5 ± 0.5 μm thick, and its XRD pattern, Fig. 4a, features broad bands

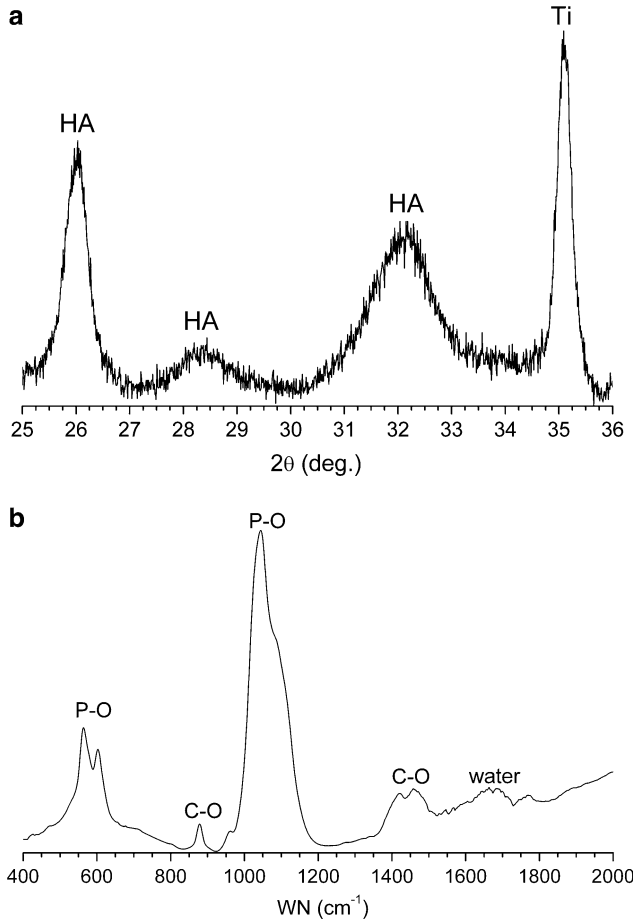

Fig. 4 XRD pattern (**a**) and FTIR absorbance spectrum (**b**) of Ca–P layer formed on Ti wire after soaking in SBF1 for 24 h

typical of nano-crystalline hydroxyapatite [18]. Characteristic splitting of the orthophosphate absorption bands at 600–560 cm^{-1} in the FTIR spectrum, Fig. 4b, confirms the crystalline nature of the layer [19]. In addition, carbonate bands can be detected in the spectrum suggesting the formation of carbonated nanocrystalline HA (nano-CHA). Similar nanocrystalline HA layers with grain size less than 20 nm were reported for electrochemically alkali-treated Ti6Al4V samples immersed in simulated body fluid with Ca^{2+} and HPO_4^{2-} concentrations enhanced by a factor of five [20].

3.3 Soaking 0.2 mm diam. Ti wires in SBF2

Soaking SBF1-primed 0.2-mm-diam. wires in SBF2 (Experiment 1) for relatively short time periods (4 and 8 h) resulted in the formation of a finely porous uniform Ca phosphate layer on top of the preformed nano-CHA, Fig. 5a, c. According to the XRD analysis, the layer is a single-phase hydroxyapatite, HA, Fig. 6a. After longer immersions in SBF2 (16 and 24 h), an additional layer

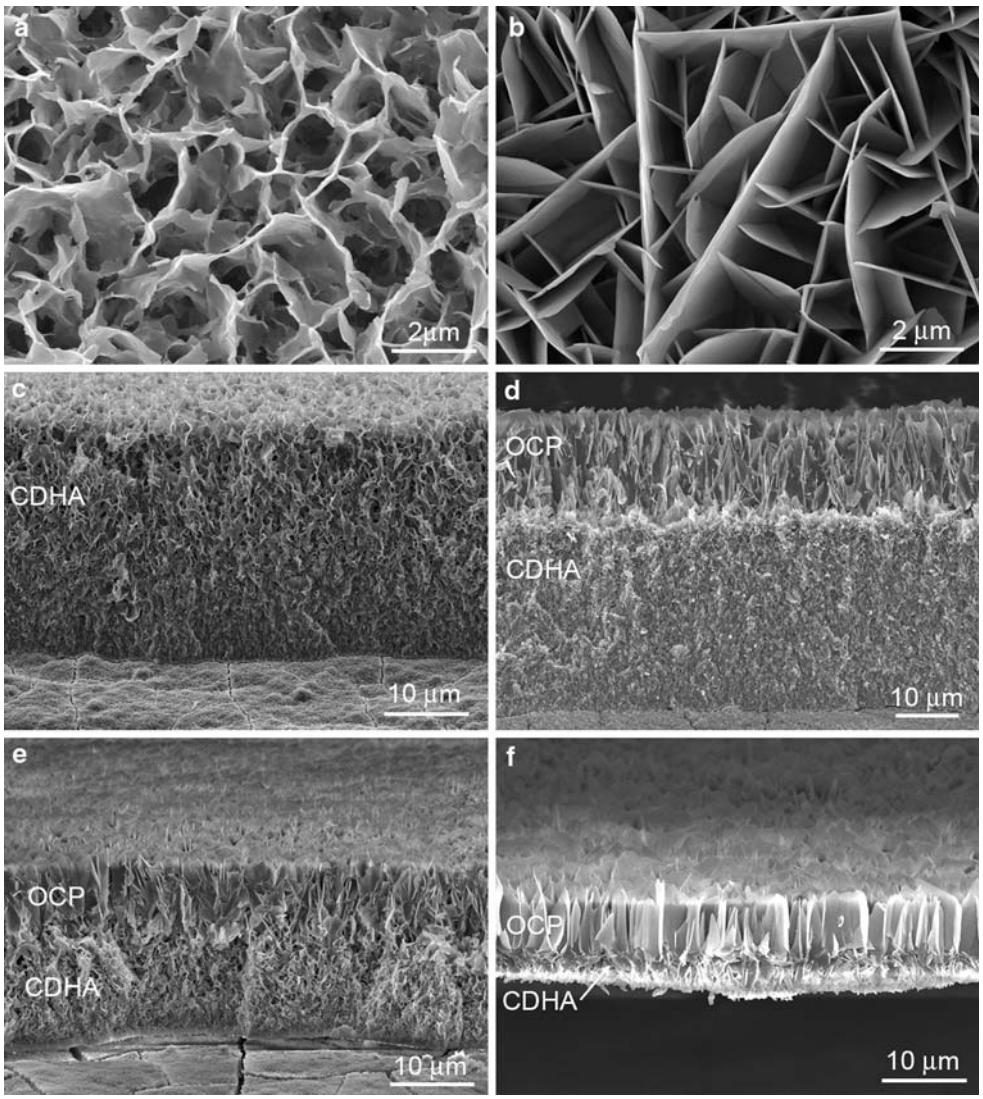

Fig. 5 HRSEM micrographs of Ca–P coatings obtained on SBF1-primed Ti substrates after soaking in SBF2 (Experiment 1): **a**,**c**—0.2-mm-diam. wire, 8 h; **b**,**d**—0.2-mm-diam. wire, 24 h; **e**—1-mm-diam. wire, 8 h; **f**—flat coupon (foil), 8 h. **a**,**b**—plan-view; **c**–**f**—cross-section. Note the same magnification in **c**, **e** and **f**

started to grow on top of the HA, Fig. 5b, d. This layer has a plate-like morphology, distinctly different from that of HA both in the plan-view and cross-section. As estimated by EDS, the Ca/P ratio of the surface (plate-like) layer was somewhat lower than that of the HA layer underneath. XRD pattern of the wires with the two-layer Ca–P coating, Fig. 6b, contains, in addition to the HA peaks, several characteristic peaks of octacalcium phosphate, OCP, suggesting that the topmost layer with the plate-like morphology is OCP. FTIR spectra in Fig. 7 confirm the XRD results, as the 1030–1130 cm^{-1} orthophosphate (P–O) band shows a more distinct separation of peaks after 24 h deposition (Fig. 7b) than after 8 h deposition (Fig. 7a) due to the presence of OCP in the former coating [19]. The P–OH peaks corresponding to bivalent phosphate, HPO_4^{2-} (at 870 and 920 cm^{-1}) are detected in the spectrum of the single-phase HA coating (8 h deposition) suggesting that the HA formed is a Ca-deficient compound, $Ca_{10-x}(HPO_4)_x(PO_4)_{6-x}(OH)_{2-x}$ (CDHA). Unlike its stoichiometric counterpart, $Ca_{10}(PO_4)_6(OH)_2$, CDHA is soluble in the body fluids, and its solubility increases dramatically with decreasing Ca/P ratio [21]. CDHA is indistinguishable from the stoichiometric HA by XRD analysis, however, unlike the stoichiometric HA, it will decompose on heating to 740°C into β-tricalcium phosphate, $Ca_3(PO_4)_2$ (β-TCP) and stoichiometric HA according to the reaction [22]:

$$Ca_{10-x}(HPO_4)_x(PO_4)_{6-x}(OH)_{2-x} \rightarrow (1-x)Ca_{10}(PO_4)_6(OH)_2 + 3xCa_3(PO_4)_2 + xH_2O \quad (1)$$

The XRD pattern of HA-coated Ti wire (8 h in SBF2) annealed at 740°C for 30 min is shown in Fig. 8. The only phase detected is β-TCP implying that the HA layer is Ca-deficient with x value close to unity:

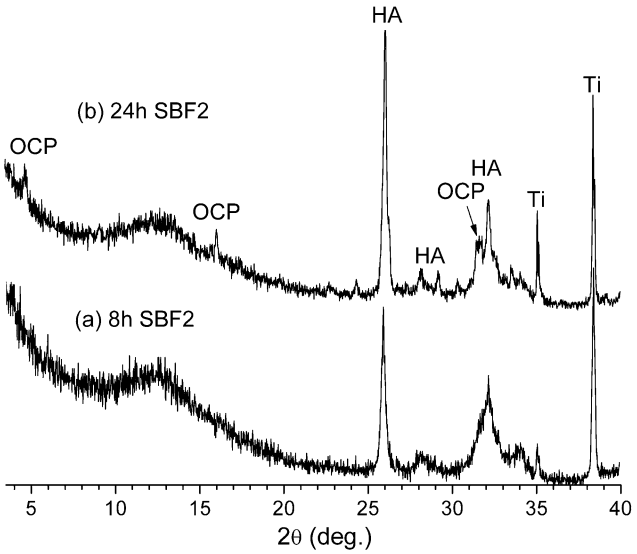

Fig. 6 XRD patterns of SBF1-primed Ti wires after 8 h (**a**) and 24 h (**b**) soaking in SBF2 Note the absence of OCP peaks in **a**

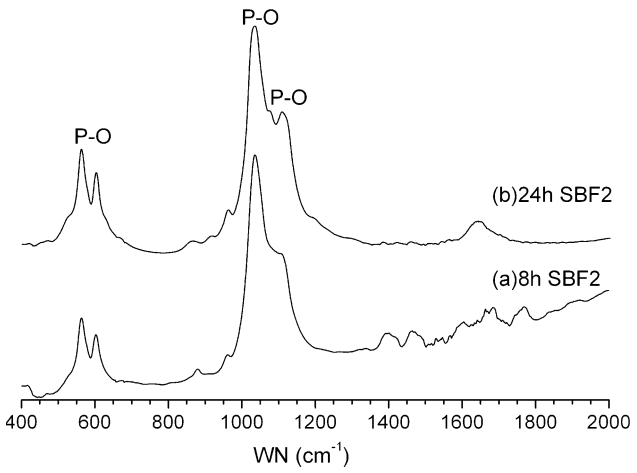

Fig. 7 FTIR absorbance spectra of Ca–P coatings obtained after 8 h (**a**) and 24 h (**b**) soaking in SBF2

$Ca_9(HPO_4)(PO_4)_5(OH)$. The Ca/P ratio of such CDHA is ~1.5, and its solubility is comparable to that of β-TCP [23].

As can be seen in Fig. 9, the CDHA layer on 0.2-mm-diam. wires grows almost linearly, and its growth stops when the OCP layer starts to form. The growth rate of OCP decreases with time and practically no layer thickening is observed after 24 h deposition. By the end of this period, the pH of SBF2 drops from 7.2 to ~6.9. Both the CDHA and OCP layers were found to be very porous, with the apparent density of 0.85 and 0.60 g/cm^3, respectively, which corresponds to ~70% porosity for CDHA and ~80% porosity for OCP.

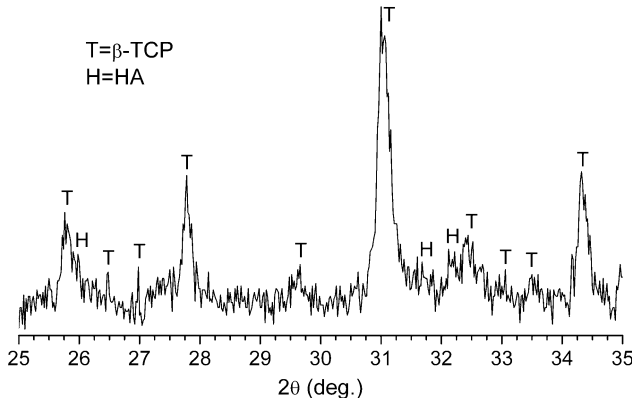

Fig. 8 XRD pattern of SBF1-primed Ti wires soaked in SBF2 for 8 h and annealed at 740°C, 30 min. Decomposition to β-TCP upon annealing indicates that the initial HA layer is Ca-deficient

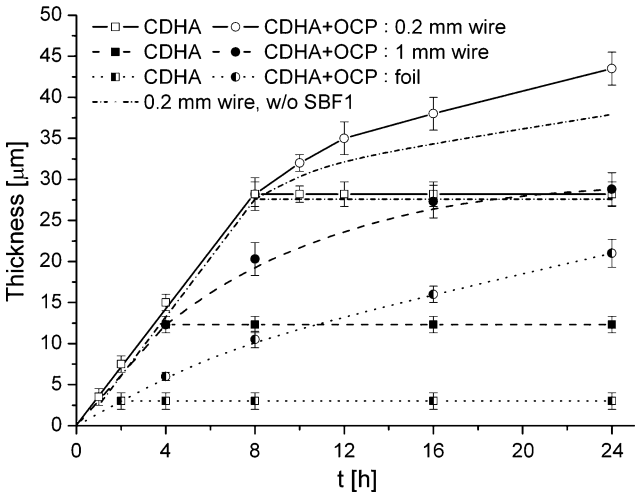

Fig. 9 Thickness of the CDHA layer and of the entire CDHA + OCP coating on SBF1-primed 0.2-mm-diam. (*solid lines*) and 1-mm-diam. (*dashed lines*) Ti wires, on SBF1-primed Ti foils (*dotted lines*) and on 0.2-mm-diam. Ti wires non-primed in SBF1 (*dash-dot lines*) versus immersion time in SBF2

Soaking bare alkali-treated 0.2-mm-diam. wires (not primed in SBF1) in SBF2 for up to 24 h yielded Ca–P coatings similar to those grown on the SBF1-primed wires. The thickness and growth kinetics of Ca–P coatings on the two types of wires were almost identical, Fig. 9.

Increasing the acidity of SBF2 (by adding HCl) resulted in the formation of thinner coatings on wires with less HA and more OCP: (12 μm HA + 16 μm OCP) and (1 μm HA + 25 μm OCP) after 24 h deposition at pH 7.0 and 6.8, respectively. Decreasing the concentration of Ca^{2+} in SBF2 from 4 to 3.5 mM had a similar effect yielding (24 μm HA + 13 μm OCP) after 24 h immersion. No continuous coating was formed at Ca^{2+} concentration of 3 mM with separate islands of OCP observed on the wire surface.

3.4 0.2 mm versus 1 mm diam. wires versus flat coupons

The growth of CaP coating on a 1-mm-diam. wire or a flat coupon (foil) immersed separately in SBF2 (experiment 1) followed the same pattern as for the 0.2-mm-diam. wire albeit at a measurably slower pace, Fig. 9. It can be seen that at any time point, coating thicknesses, b, are related as $b_{0.2} > b_1 > b_{flat}$. The smaller the curvature, the sooner the OCP layer starts to form: after 8 h soaking, no OCP layer is detected on a 0.2-mm-diam. wire whereas such a layer is clearly seen on a 1-mm-diam. wire, Fig. 5e. On a flat surface, the OCP layer starts to appear even earlier and constitutes, after 8 h soaking, the major component of the coating, Fig. 5f.

The effect of surface curvature was also clearly observed when a 0.2-mm-wire and a flat coupon were immersed together in SBF2 (Experiment 2). It can be seen in Fig. 10 that despite being immersed in the same solution, the coatings on the wire and flat surface differ both in thickness and interrelation of the HA and OCP phases: the coatings on flat are thinner and have a significantly lower proportion of the HA phase.

When Experiment 2 was conducted in the agitated SBF2 solution, single-phase HA coatings of comparable thickness were obtained on both foil and wire. No OCP layer was detected even after 4 days immersion.

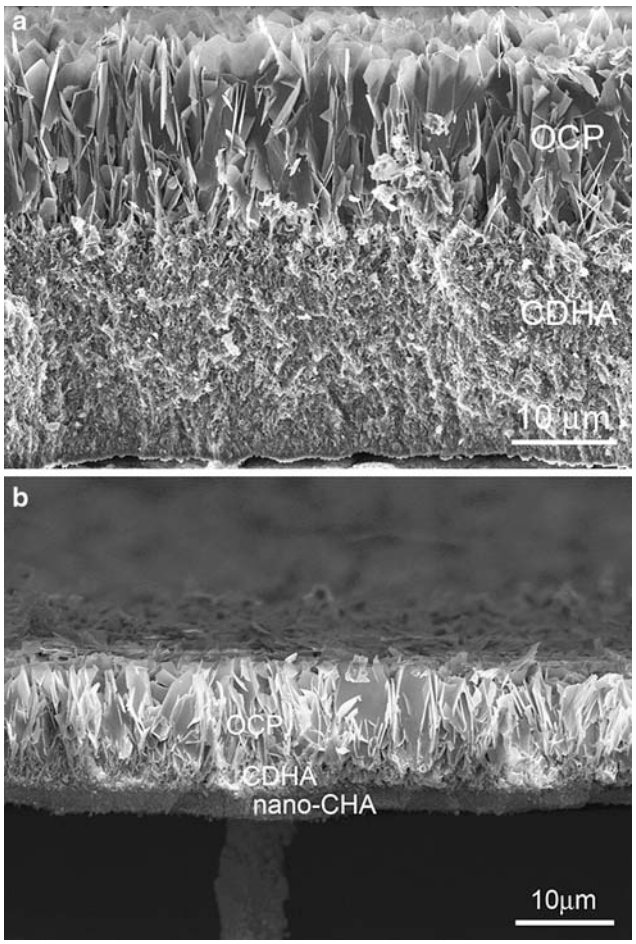

Fig. 10 Cross-section HRSEM micrographs of Ca–P coatings on SBF1-primed 0.2-mm-diam. wire (**a**) and flat coupon (**b**) soaked together in SBF2 for 24 (Experiment 2). Note the smaller coating thickness and the lower fraction of CDHA on the coupon

4 Discussion

Biomimetic coatings of different thickness and composition were grown on Ti substrates, depending on surface geometry and deposition conditions (pH and $[Ca^{2+}]$ of SBF2 and stirring). After 24 h soaking in non-agitated SBF2 (pH 7.2), the coatings consisted of two distinct layers: the surface layer of large plate-like OCP and the fine-grained layer of Ca-deficient hydroxyapatite (HA) underneath. Such double-layer HA/OCP coatings were formed on SBF1-primed plates and wires (on top of the preformed nano-CHA film), as well as on bare alkali-treated wires. The HA layer is the first to be formed since it is the only one observed after short soaking times (up to 8 h for wires and up to 1 h for plates). At the later stages, the growth of HA is halted and the OCP layer starts to grow, apparently due to some change in the precipitation conditions. The early formation of the thermodynamically stable apatite phase seemingly contradicts the well known fact that in solutions supersaturated with respect to both HA and OCP, the precipitation of OCP is kinetically favored [24]. It has been reported by many authors that HA wouldn't form directly from solution but only via a precursor, with OCP often suggested as a transitional state during the formation of HA, both in biological mineralization and in vitro [24, 25]. It is, therefore, believed that in our case, too, the apatite phase is not precipitated directly from the solution but through the OCP intermediate. To explain the early formation of the HA layer, the following mechanism of biomimetic deposition is proposed. The process starts with the formation of OCP according to [7]:

$$8Ca^{2+} + 6HPO_4^{2-} + 5H_2O \rightarrow Ca_8H_2(PO_4)_6{\cdot}5H_2O + 4H^+ \quad (2)$$

We hypothesize that initially the SBF2 solution is highly supersaturated with respect to OCP: the nucleation rate is higher than the crystal growth rate and OCP precipitation is dominated by nucleation. As a result, a large amount of very fine OCP crystals are formed that are transformed into HA by a hydrolysis reaction [26]:

$$Ca_8H_2(PO_4)_6{\cdot}5H_2O + 2Ca^{2+} \rightarrow Ca_{10}(PO_4)_6(OH)_2 + 3H_2O + 4H^+ \quad (3)$$

Due to their nanometer size and plate-like shape, the hydrolytic conversion of OCP crystals into HA is very rapid and complete, so that no traces of OCP are detected in the corresponding XRD patterns (e.g. Fig. 6a). Similarly to many previous reports [27–29], the product of OCP hydrolysis in our case has a Ca/P ratio lower than that of the stoichiometric HA. Both the precipitation of OCP intermediate and its hydrolysis into HA according to the above reactions acidify the solution (produce H^+) which is consistent with the pH decrease measured in our experiments. The gradual thickening of the HA layer leads to depletion of Ca^{2+} ions from the solution which, together with the lower pH, makes the solution less supersaturated with respect to OCP. Both the nucleation and crystal growth rates decrease with decreasing supersaturation, the effect being much stronger for the nucleation rate [30]. Eventually, a certain critical supersaturation, S_{cr}, is reached where the nucleation of OCP becomes impossible and crystal growth becomes the dominant mechanism of OCP formation. The growing OCP crystals with typical plate-like morphology [31] constitute the second layer of the biomimetic coating. The hydrolytic transformation of large OCP plates into HA becomes difficult because of the slow kinetics of reaction (3) consisting of calcium diffusion into the hydrolyzing crystal and the removal of water molecules [25], as well as the depletion of Ca^{2+} ions required for the reaction. Nevertheless, it is reasonable to believe that some hydrolysis takes place and that the large plate-like crystals consist of OCP in the central part and a thin layer of HA on the surface. This assumption is supported by the low intensity of the OCP peaks in XRD patterns of coatings with thick 'OCP' layers (e.g. Fig. 6b). To summarize, the growth of fine-grained Ca-deficient HA layer continues as long as the supersaturation of SBF2 is sufficiently high for OCP precipitation, and it gives way to the growth of plate-like OCP when the supersaturation drops below a certain critical value.

The proposed mechanism of the two-layer HA-OCP coating formation is confirmed by the results of immersions in SBF2 solutions with lower initial pH or lower $[Ca^{2+}]$. Given the fact that the solubility of Ca–P compounds depends on acidity, the supersaturation of precipitating solution with respect to OCP can be controlled not only by the Ca^{2+} content but also by pH [32, 33]. SBF solutions with lower $[Ca^{2+}]$ or lower pH are less supersaturated and thus should favor OCP crystal growth over nucleation. Indeed, thinner HA layers (growing by nucleation and subsequent hydrolysis of OCP) and correspondingly thicker plate-like OCP layers were observed when biomimetic deposition was conducted at $[Ca^{2+}] < 4$ mM (3.5 and 3 mM) or pH < 7.2 (7 and 6.8). Stirring the supersaturated SBF2 solution enhances nucleation rate and disrupts crystal growth [34] thus leading to the formation of a single fine-grained HA layer.

As mentioned above, thick biomimetic Ca–P coatings can be grown on alkali-treated Ti wires even without priming in SBF1. The main difference in the kinetics of Ca–P growth on SBF1-primed and on bare alkali-treated Ti wires is the presence of a short incubation period in the latter case, Fig. 9.

The markedly different results obtained for wires of different diameter and flat coupons having the same total surface area, and for wires and flat coupons immersed together in SBF2 suggest that the growth of Ca–P layer is controlled not only by the general supersaturation of the immersion solution but by the local supersaturation at the substrate surface as well. Since the surface area per unit length of the 1-mm-diam. wire is larger than that of the 0.2-mm-diam. wire, more Ca^{2+} and phosphate ions are required to build a Ca–P layer of a fixed thickness on the 1-mm-diam. wire. As a result, the solution around the 1-mm-diam. wire is depleted of these ions faster and Ca^{2+} concentration drops to the critical supersaturation degree, S_{cr}, sooner than around the 0.2-mm-diam. wire. This explains why the OCP layer on the 1-mm-diam. wire is observed after shorter immersions than for the 0.2-mm-wire. A flat coupon may be considered as a wire with infinite diameter, therefore S_{cr} is reached even faster and there is hardly time for a layer of HA (hydrolyzed nanoscale OCP) to be formed before the layer of plate-like OCP starts to grow. It must be for this reason coupled with the lower pH (7.05) that no HA layer was observed by Barrère et al. [7] on Ti6Al4V plates following immersion in SBF2. Agitating the SBF2 solution eliminates concentration gradients, enhances nucleation rate and disrupts crystal growth, which leads to the formation of similar single-phase HA layers on both Ti wires and flat samples. It is worth noting that different crystallization conditions (and, possibly, other coating morphologies) could be expected for porous scaffolds that are built of a large number of wire-like struts and have much more surface area than a single wire.

5 Conclusions

The main thrust of the present work was to compare the structure of biomimetic calcium phosphate coatings on Ti wires of different diameter and on flat Ti coupons. The results show that different calcium phosphate phases having different solubilities in the body fluids, different surface morphology and correspondingly different bone-building potentials can be obtained depending on the substrate

geometry and deposition time. The main conclusions are as follows:

1. The phase composition of biomimetic Ca–P coatings deposited on alkali treated thin wires is different from those deposited on similarly pretreated flat coupons. While the coatings on flat surfaces are comprised almost entirely of plate-like octacalcium phosphate (OCP), the coatings on wires consist of a fine-grained hydroxyapatite (HA) layer after short deposition times, and of a layer of plate-like OCP on top of the HA layer after longer immersions.
2. Biomimetic Ca–P coatings on thin wires grow faster and are thicker than the corresponding coatings on flat coupons.
3. The hydroxyapatite layer on wires and on flat coupons is Ca-deficient with the composition close to tricalcium phosphate (TCP).
4. According to the proposed mechanism, biomimetic deposition of Ca–P proceeds in three stages: (1) precipitation of the kinetically favored OCP phase under rapid nucleation conditions (high initial supersaturation); (2) instantaneous hydrolysis of very fine OCP crystallites into a more stable Ca-deficient HA phase; (3) OCP crystal growth under slow nucleation conditions. Stage (3) starts when supersaturation drops below a certain value due to depletion of Ca^{2+} from the solution and a drop in pH value leading to the formation of large OCP plates stable towards further hydrolysis to HA. The difference in thickness and in OCP/HA proportion for biomimetic Ca–P coatings on wires with different diameters and flat coupons is explained by different local supersaturation conditions at the solution/Ca–P layer interface.

Acknowledgements This work was supported by Israel Science Foundation (ISF) through research grant No. 1193/05, by the Commission of the European Communities, Network of Excellence (EXCELL) No. 515703, and by Israel Ministry of Science, Culture and Sport in the frames of the Fellowship Program for Advancement of Women in Science. The authors are grateful to Prof. E.Y. Gutmanas, Faculty of Materials Engineering, Technion, for his assistance and fruitful discussions.

References

1. Jaffe WL, Scott DF. Current concepts review: total hip arthroplasty with hydroxyapatite-coated prostheses. J Bone Joint Surg. 1996;78:1918–34.
2. Shepperd JAN, Apthorp H. A contemporary snapshot of the use of hydroxyapatite coating in orthopaedic surgery. J Bone Joint Surg [Br]. 2005;87-B:1046–9.
3. Mao C, Li H, Cui F, Ma C, Feng Q. Oriented growth of phosphates on polycrystalline titanium in a process mimicking biomineralization. J Crystal Growth. 1999;206:308–21.
4. Li F, Feng QL, Cui FZ, Li HD, Schubert H. A simple biomimetic method for calcium phosphate coating. Surf Coat Technol. 2002;154:88–93.
5. Zhang Q, Leng Y, Xin R. A comparative study of electrochemical deposition and biomimetic deposition of calcium phosphate on porous titanium. Biomaterials. 2005;26:2857–65.
6. Yan WQ, Nakamura T, Kawanabe K, Nishigochi S, Oka M, Kokubo T. Apatite layer-coated titanium for use as bone bonding implants. Biomaterials. 1997;18:1185–90.
7. Barrère F, Layrolle P, van Blitterswijk CA, de Groot K. Biomimetic coatings on titanium: a crystal growth study of octacalcium phosphate. J Mater Sci: Mater Med. 2001;12:529–34.
8. Barrère F, Layrolle P, van Blitterswijk CA, de Groot K. Biomimetic calcium phosphate coatings on Ti6Al4 V: a crystal growth study of octacalcium phosphate and inhibition by Mg^{2+} and HCO_3. Bone. 1999;25:107S–11S.
9. Habibovic P, Barrère F, van Blitterswijk CA, de Groot K, Layrolle P. Biomimetic hydroxyapatite coating on metal implants. J Am Ceram Soc. 2002;85:517–22.
10. Sovak G, Weiss A, Gotman I. Osseointegration of Ti-6Al-4 V alloy implants with a novel titanium nitride coating in the rat femur. J Bone Joint Surg [Br]. 2000;82-B:290–6.
11. Rammelt S, Schulze E, Bernhardt R, Hanisch U, Scharnweber D, Worch H, et al. Coating of titanium implants with type-I collagen. J Orthop Res. 2004;22:1025–34.
12. Rammelt S, Illert T, Bierbaum S, Scharnweber D, Zwipp H, Schneiders W. Coating of titanium implants with collagen, RGD peptide and chondroitin sulfate. Biomaterials. 2006;27:5561–71.
13. Akca K, Sarac E, Baysal U, Fanuscu M, Chang T-L, Cehreli M. Micro-morphologic changes around biophysically-stimulated titanium implants in ovariectomized rats. Head Face Med. 2007;3:28–34.
14. Ito S, Takebe J. Longitudinal observation of thin hydroxyapatite layers formed on anodic oxide titanium implants after hydrothermal treatment in a rat maxilla model. Prosthodont Res Pract. 2008;7:82–8.
15. Li P, Ohtsuki C, Kokubo T, Nakanishi K, Soga N, De Groot K. The role of hydrated silica, titania, and alumina in inducing apatite on implants. J Biomed Mater Res. 1994;28:7–15.
16. Kim HM, Miyaji F, Kokubo T, Nishiguchi S, Nakamura T. Graded surface structure of bioactive titanium prepared by chemical treatment. J Biomed Mater Res. 1999;45:100–7.
17. Feng QL, Wang H, Cui FZ, Kim TN. Controlled crystal growth of calcium phosphate on titanium surface by NaOH-treatment. J Crystal Growth. 1999;200:550–7.
18. Drouet C, Bosc F, Banu M, Largeot C, Combes C, Dechambre G, et al. Nanocrystalline apatites: from powders to biomaterials. Powder Technol. 2009;190:118–22.
19. Sauer GR, Wuthier RE. Fourier transform infrared characterization of mineral phases formed during induction of mineralization by collagenase-released matrix vesicles in vitro. J Bio Chem. 1988;263:13718–24.
20. Xie J, Luan BL. Nanometer-scale surface modification of Ti6Al4V alloy for orthopedic applications. J Biomed Mater Res. 2008;84A:63–72.
21. Mavropoulos E, Rossi AM, Da Rocha NCC, Soares GA, Moreira JC, Moure GT. Dissolution of calcium-deficient hydroxyapatite synthesized at different conditions. Mater Character. 2003;50:203–7.
22. Ishikawa K, Ducheyne P, Radin S. Determination of the Ca/P ratio in calcium-deficient hydroxyapatite using X-ray diffraction analysis. J Mater Sci: Mater Med. 1993;4:165–8.
23. Bohner M. Calcium orthophosphates in medicine: from ceramics to calcium phosphate cements. Injury. 2000;31:S-D37–47.

24. Brown WE, Eidelman N, Tomazic B. Octacalcium phosphate as a precursor in biomineral formation. Adv Dent Res. 1987;1:306–13.
25. Bodier-Houllé P, Steuer P, Voegel JC, Cuisinier FJG. First experimental evidence for human dentine crystal formation involving conversion of octacalcium phosphate to hydroxyapatite. Acta Cryst. 1998;D54:1377–81.
26. Elliott JC. Structure and chemistry of the apatite and other calcium orthophosphates. Amsterdam: Elsevier; 1994.
27. LeGeros RZ, Daculsi G, Orly I, Abergas T, Torres W. Solution-mediated transformation of octacalcium phosphate (OCP) to apatite. Scan Micr. 1989;3:129–38.
28. Suzuki O, Kamakura S, Katagiri T, Nakamura M, Zhao B, Honda Y, et al. Bone formation enhanced by implanted octacalcium phosphate involving conversion into Ca-deficient hydroxyapatite. Biomaterials. 2006;27:2671–81.
29. Nelson DGA, McLean JD. High-resolution electron microscopy of octacalcium phosphate and its hydrolysis products. Calcif Tissue Int. 1984;36:219–32.
30. Nývlt J, Söhnel O, Matuchová M, Broul M. The kinetics of industrial crystallization. Prague: Academia Prague; 1985.
31. Terpstra RA, Bennema P. Crystal morphology of octacalcium phosphate: theory and observation. J Crystal Growth. 1987; 82:416–26.
32. Shirkhanzadeh M. Direct formation of nanophase hydroxyapatite on cathodically polarized electrodes. J Mater Sci: Mater Med. 1998;9:67–72.
33. Savvin Yu N, Kryzhanovskaya AS, Tolmachev AV. Effect of growth conditions on the structural properties of calcium phosphate coatings prepared in the system $CaCl_2$–KH_2PO_4–KOH–HCl–H_2O. Inorg Mater. 2005;41:864–8.
34. Mullin JW, Raven KD. Nucleation in agitated solutions. Nature. 1961;190:251.